SUPPLEMENTARY INFORMATION

Supplementary Table 1. Properties of CF4 and Ctrl-CF4-S2

	Cu^+	Φ	λ_{em} / nm	λ_{abs} / nm	ε / $M^{-1}cm^{-1}$	Fold turn-on	K_d / M
CF4	–	0.0012	562	504, 548	3.5×10^4, 3.8×10^4	10	2.94×10^{-13}
	+	0.013	561	536	6.0×10^4		
Ctrl-CF4-S2	–	0.0056	559	503, 542	1.9×10^4, 2.2×10^4	1	N/A
	+	0.0056	559	503, 542	1.9×10^4, 2.2×10^4		

Supplementary Figures

Supplementary Figure 1. CF4 response to Cu^+.

Fluorescence response of 1 μM CF4 to Cu^+. Spectra shown are for [Cu^+] of 0, 0.2, 0.4, 0.6, 10.8, 1.0 and 1.2 μM. These experiments have been repeated independently 3 times with similar results.

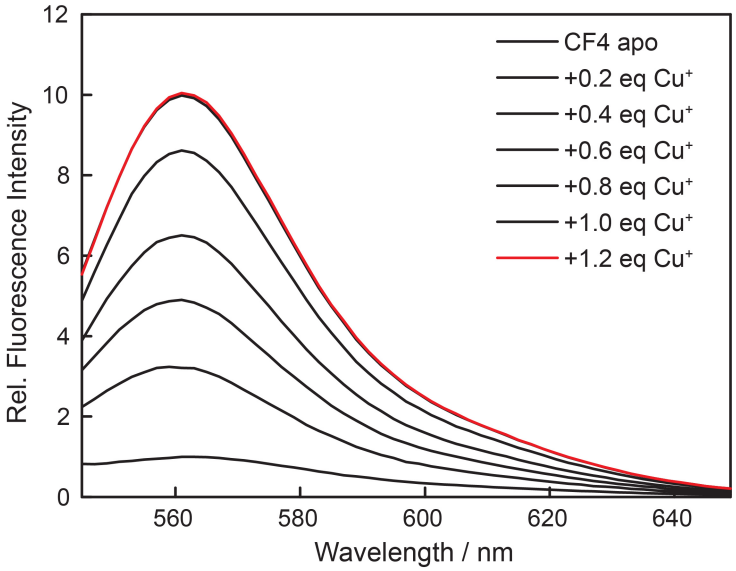

Supplementary Figure 2. Characterization of CF4

(a) UV-visible spectral change of 2 μM CF4 upon addition of 2 μM Cu^+. (b) Job's plot of CF4 and Cu^+. The total combined concentration of CF4 and Cu^+ was kept at 1 μM. (c) Fluorescence responses of 1 μM CF4 to thiourea-buffered Cu^+ solutions for K_d measurement. The observed

K_d value is 2.9×10^{-13} M. Solid line represents the calculated curve. (d) In vitro spectroscopic characterization of effect of pH on fluorescence of both apo and Cu^+-bound CF4 in buffers prepared by neutralizing the free acid solutions of 25 mM HEPES, 25 mM MES and 25 mM acetic acid with 5 M NaOH. These experiments have been repeated independently 3 times with similar results.

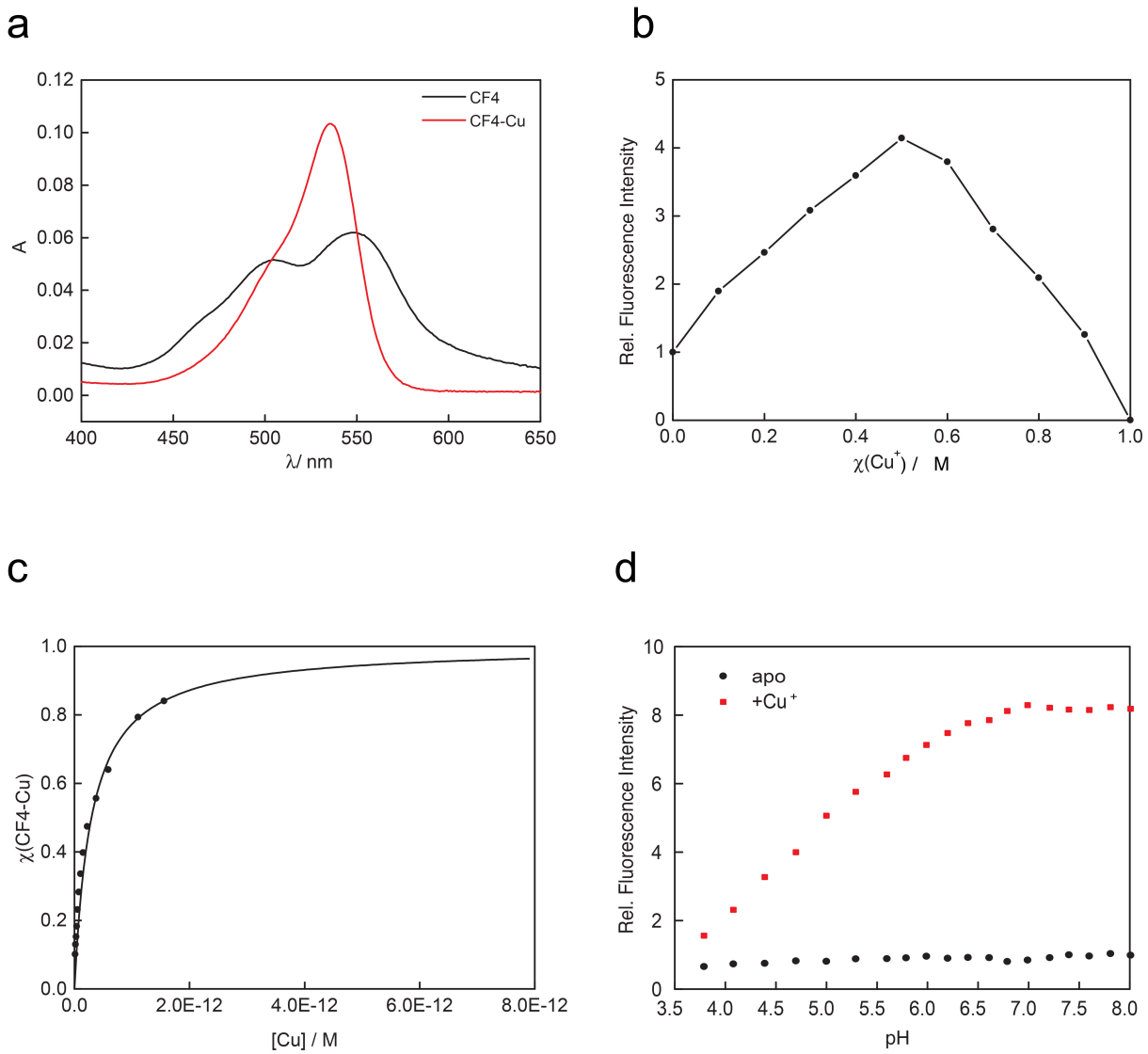

Supplementary Figure 3. Characterization of Ctrl-CF4-S2

(a) Fluorescence response of 1 μM Ctrl-CF4-S2 to Cu^{+}. Spectra shown are for [Cu^{+}] of 0, 0.2, 0.4, 0.6, 0.8, 1.0 and 1.2 μM. (b) Fluorescence responses of Ctrl-CF4-S2 to various metal ions. Bars represent the final integrated fluorescence response (F_f) over the initial integrated emission (F_i). Grey bars represent the addition of an excess of the indicated metal ion (2 mM for Na^{+}, Mg^{2+}, K^{+}, Ca^{2+}, and Zn^{2+}, 50 μM for all other cations) to a 2 μM solution of Ctrl-CF4-S2. Red bars represent the subsequent addition of 2.5 μM Cu^{+} to the solution. (c) UV-visible spectral change of 2 μM Ctrl-CF4-S2 upon addition of 2 μM Cu^{+}. (d) Spectroscopic characterization of effect of pH on fluorescence of Ctrl-CF4-S2 in the absence or presence of Cu^{+}. These experiments have been repeated independently 3 times with similar results.

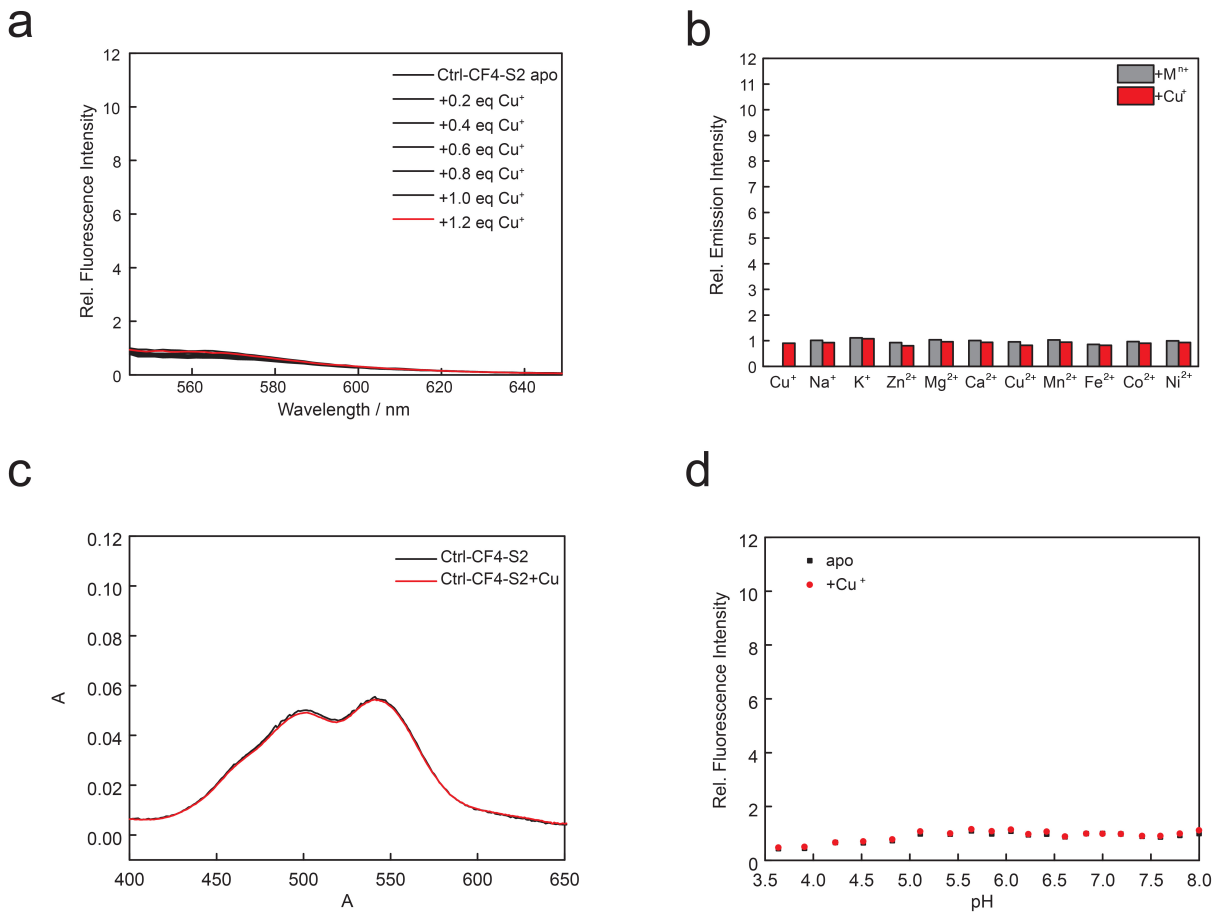

Supplementary Figure 4. Comparison of copper probe loading.

(a) to (c) are confocal images of HEK293T cells. (a) Ctrl-CF4. (b) Ctrl-CF4-S2. (c) CF4. Scale bar is 20 μm. (d) to (f) are optical sections of 3 dpf zebrafish nacre larvae. (d) Ctrl-CF4. (e) Ctrl-CF4-S2 (f) CF4. These experiments have been repeated independently 3 times with similar results. Scale bar is 100 μm.

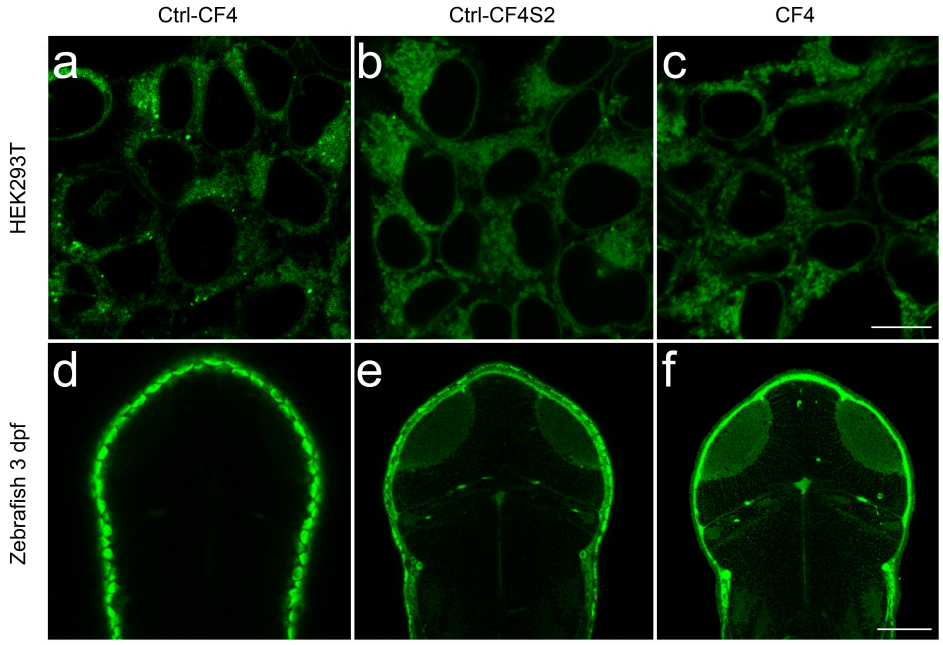

Supplementary Figure 5. Comparison of copper probes uptake in HEK293T cells.

HEK293T cells in 24-well plate were treated with CF4 or Ctrl-CF4-S2 (100 μL, 1 μM in HBSS) at 37 °C for 0.5h. The medium was then collected and extracted with 1000 μL of ethyl acetate. The fluorescence of the organic layer was measured and compared to the fluorescence of ethyl acetate extracts of probes without cell uptake to calculate the uptake ratio. Values represent average ± s.d. (n=4)

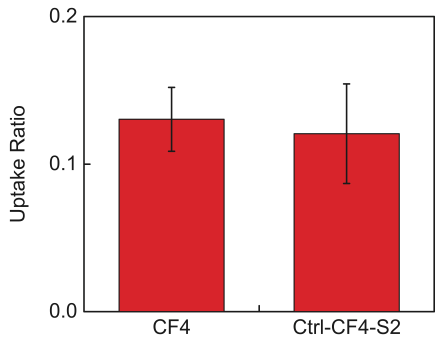

Supplementary Figure 6. In vitro characterization of CF4 and Ctrl-CF4-S2

(a) Fluorescence response of 1 μM CF4 in the presence of preformed liposomes (FormuMax, DPPC/CHOL 55:45 mol/mol, 100 nm) (grey), with subsequent addition of 1 μM Cu^{+} to the solution (red), and a final addition of 10 μM neocuproine (blue). (b) Fluorescence response of 1 μM Ctrl-CF4-S2 in the presence of preformed liposomes (FormuMax, DPPC/CHOL 55:45 mol/mol, 100 nm) (grey), with subsequent addition of 1 μM Cu^{+} to the solution (red), and a final addition of 10 μM neocuproine (blue). (c) Fluorescence response of 1 μM CF4 (grey) and Ctrl-CF4-S2 (red) in the presence of GSH, with subsequent addition of 1 μM Cu^{+} and 6 μM BCS. (d) Fluorescence response of 1 μM CF4 (grey) and Ctrl-CF4-S2 (red) to HEK293T lysates (1 mg protein/mL) and subsequent addition of 10, 50 and 100 μM Cu^{+}, followed by addition of 300 μM

BCS. These experiments have been repeated independently 3 times with similar results.

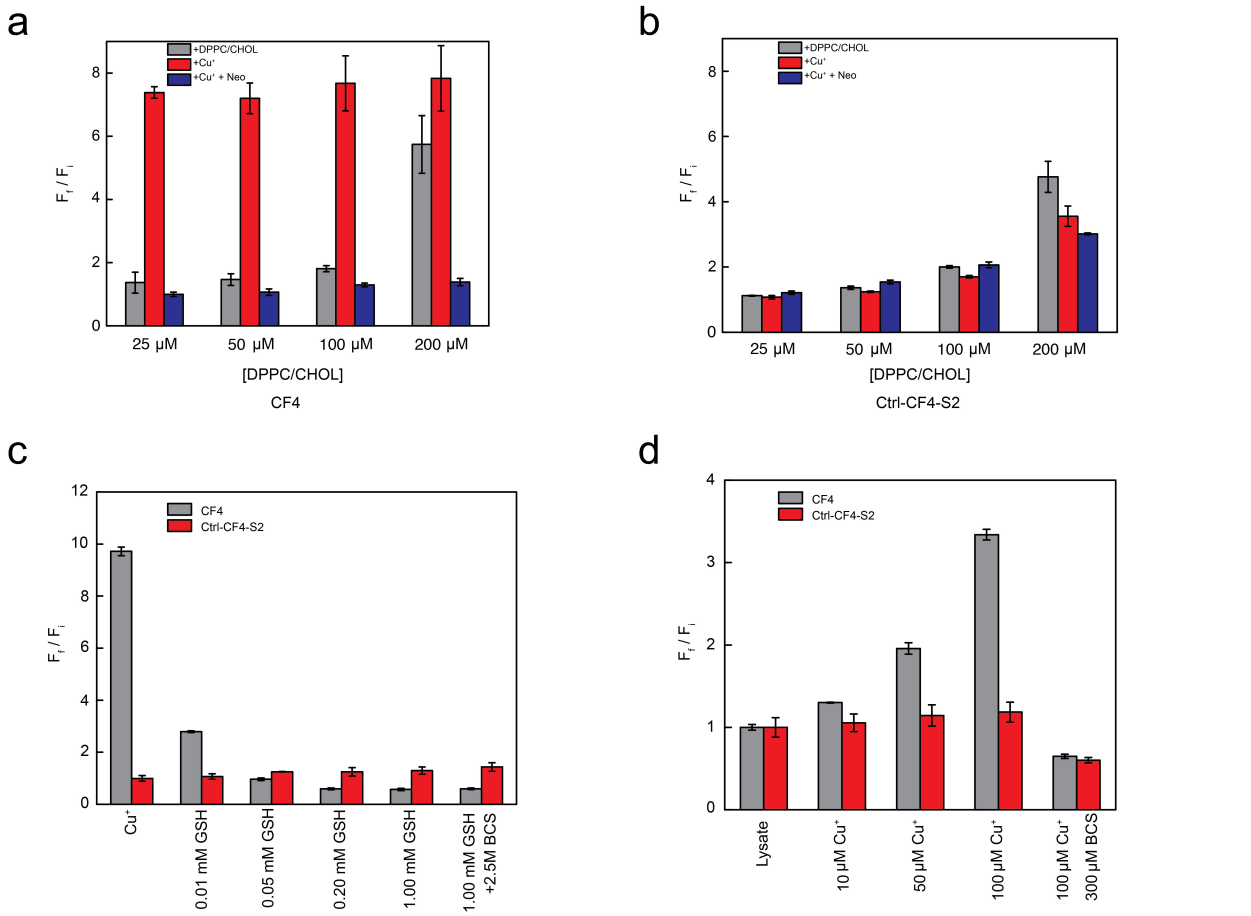

Supplementary Figure 7. CF4 responses to copper addition in HEK cells under physiological pH conditions.

Fluorescence turn-on response was measured at pH 5.5 (a), 6.5 (b), and 7.5 (c). Control HEK293T cells and HEK293T cells treated with 100 μM $CuCl_2$ for 12 h were stained with CF4 (2 μM for 10 min) dissolved in respective intracellular pH calibration buffer containing nigericin and valinomycin (ThermoFisher) and washed prior to imaging. Values represent average ± s.d. (n = 7 fields of cells per condition).

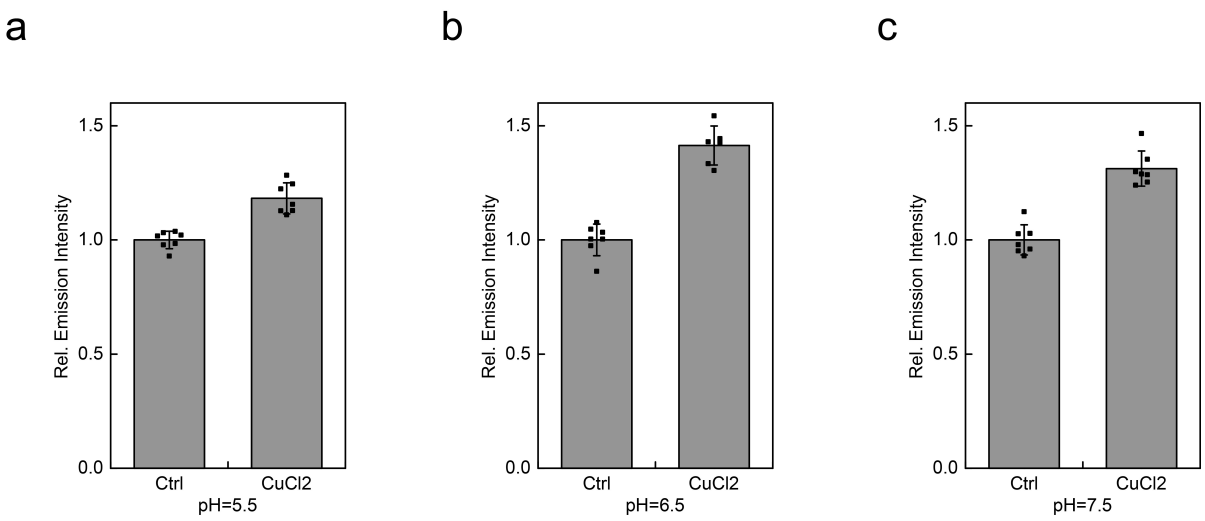

Supplementary Figure 8. LA-ICP-MS imaging reveals changes of copper distribution in the developing brain.

(a) At 2 dpf, most brain regions, including the tectum, consist of mostly cell bodies, and are not yet innervated by neurites. The lines indicate the three consecutive sections shown in (b) to (d). Panels (b) to (d) show copper distributions measured by LA-ICP-MS. (e) At 4 dpf, neurites begin to innervate brain regions, such as the tectum and cerebellum, forming neuropils, which are enriched with neurites, but depleted of cell bodies. The lines indicate the three consecutive sections shown in (f) to (h). Panels (f) to (h) show copper distributions measured by LA-ICP-MS. Scale bar is 100µm. Panels (i) to (n) show LA-ICP-MS images of *Calamity*^{gw71} mutants. Panels (i) to (k) show consecutive sections of 2 dpf larvae. Panels (l) to (n) show consecutive sections of 4 dpf larvae. Scale bar is 100 µm. T is tectum. H is Hindbrain. P → A is posterior to anterior. V → D is ventral to dorsal.The colormetric scale bar represents copper concentrations ranging from 0-1.5 ppm. N=6 independent animals imaged for each genotype with similar results.

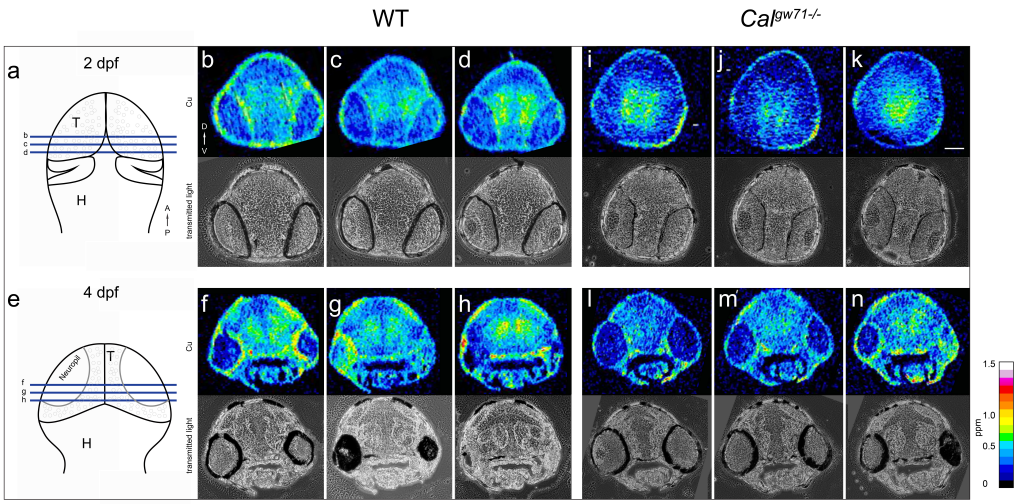

Supplementary Figure 9. Copper map in the adult zebrafish brain

The panel is a coronal section of the adult brain flash-frozen to preserve the Cu distribution. Copper distribution measured by LA-ICP-MS. (a) A schematic of adult brain with a line indicates the section in (b). TeO, optic tectum; CCe, corpus cerebelli; SRF, superior reticular formation; MLF, medial longitudinal fascicle. Scale bar is 500 μm. 5 sections from 2 brains were images with similar results.

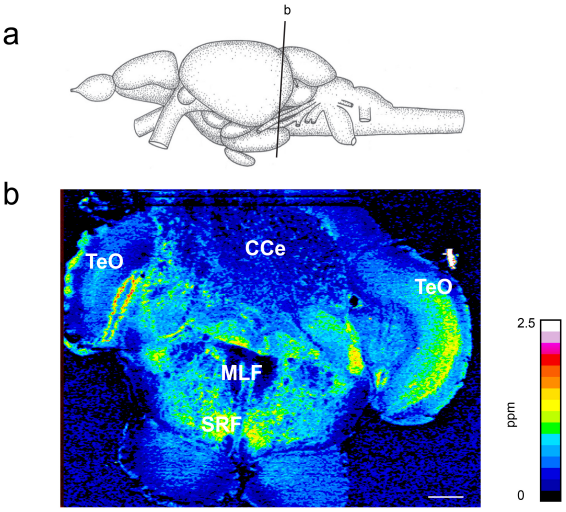

Supplementary Figure 10. WT larvae zinc map

Brain Zn distribution in larval zebrafish analyzed by LA-ICP-MS. (a) to (c) are three consecutive cross sections of 2 dpf brain. (d) to (f) are three consecutive cross sections of 4 dpf brain. (g) to (i) are three consecutive cross sections of 6 dpf brain. Scale bar is 100 μm. N=3 independent animals imaged for each genotype with similar results.

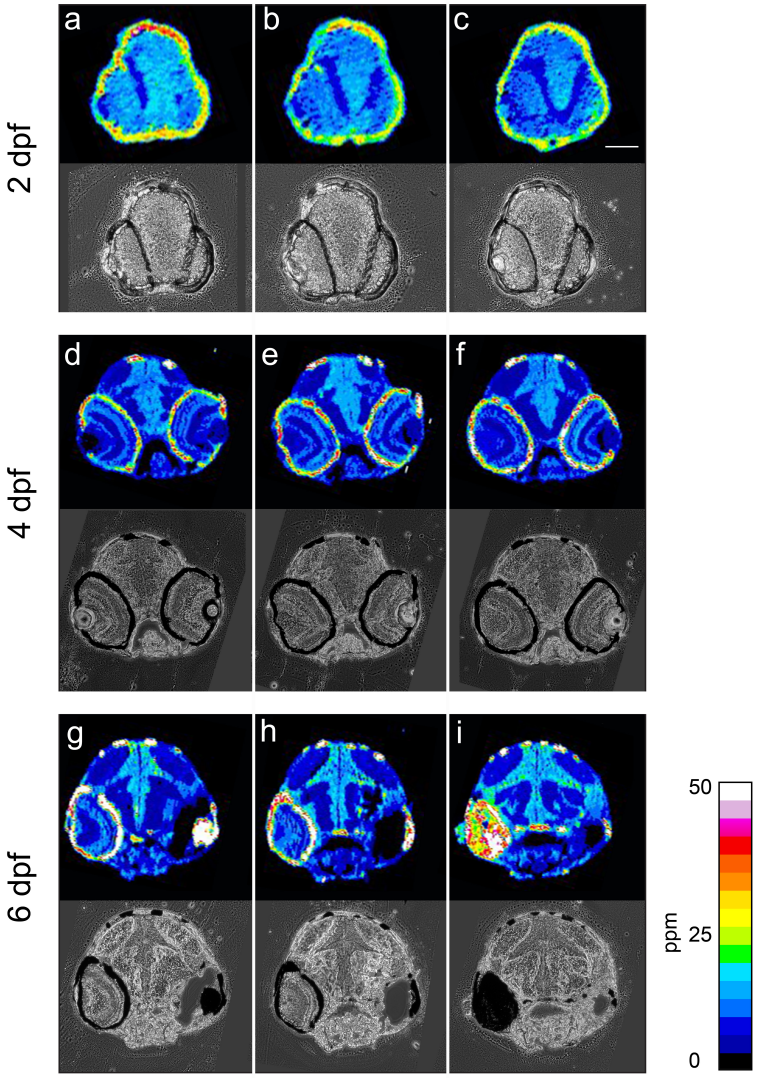

Supplementary Figure 11. *Cal*^{gw71} mutant zinc distribution is unperturbed

Brain Zn distribution in 6 dpf larval zebrafish analyzed by LA-ICP-MS. (a) to (c) are three consecutive cross sections of a *Cal*^{gw71} heterozygous brain. (d) to (f) are three consecutive cross sections of a *Cal*^{gw71} homozygous mutant brain. Scale bar is 100 μm. N=3 independent animals imaged for each genotype with similar results.

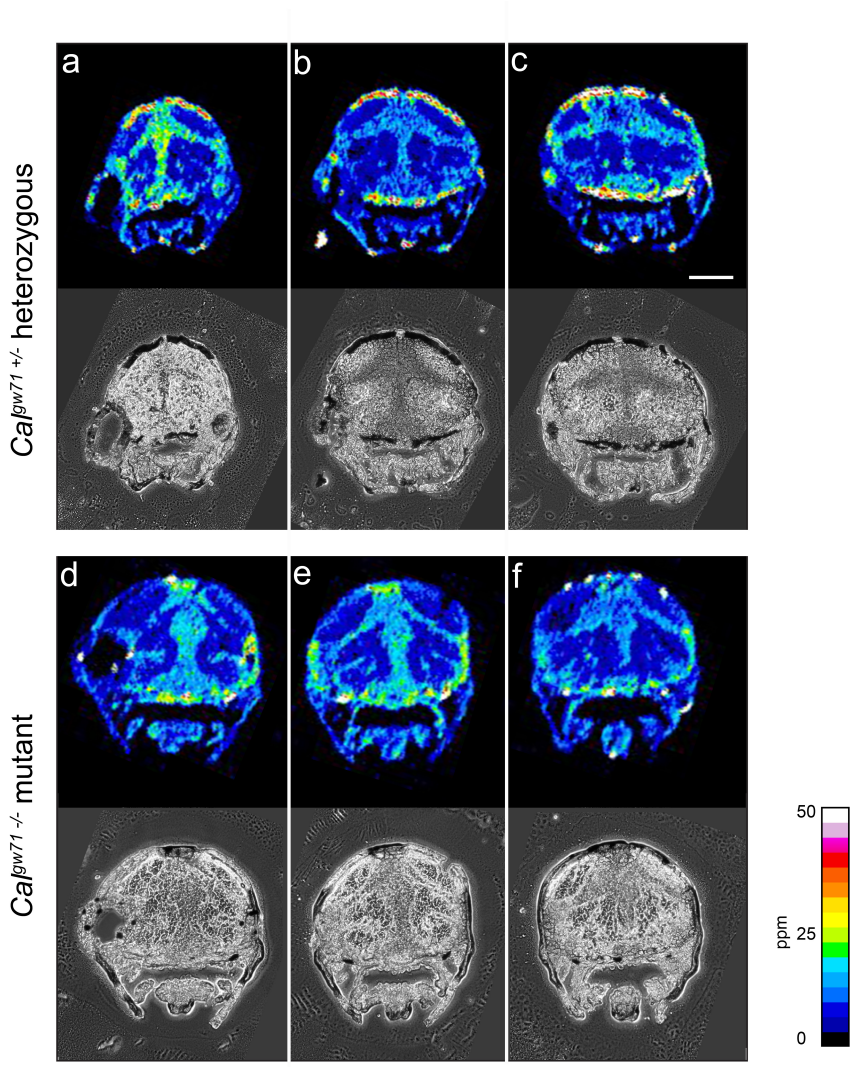

Supplementary Figure 12. Molecular imaging shows *Cal*^{gw71} mutants have lower level of labile copper in the brain.

CF4 fluorescence signals in 3 dpf WT control (a) and *Cal*^{gw71} homozygous mutant (b). Scale bar is 100μm. N=12 independent animals images in each group with similar results.

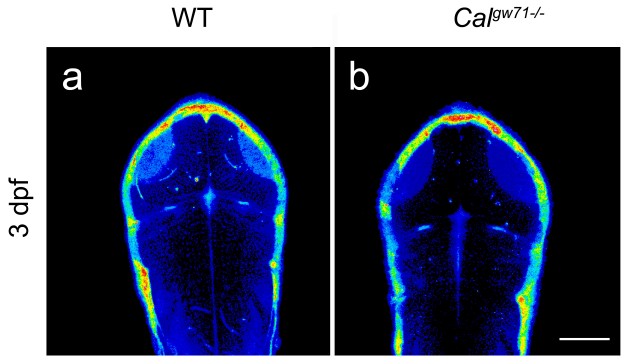

Supplementary Figure 13. *Cal*^{gw71} mutant swimming is unperturbed

Free swimming of wildtype, *Cal*$^{gw71+/-}$ and *Cal*$^{gw71-/-}$ larvae at 6 dpf. (a) The frequency of movement. (b) The speed of movement. Wildtype, N=11; *Cal*$^{gw71+/-}$, N=20; *Cal*$^{gw71-/-}$, N=12. Bars represent mean ± s.e.m.

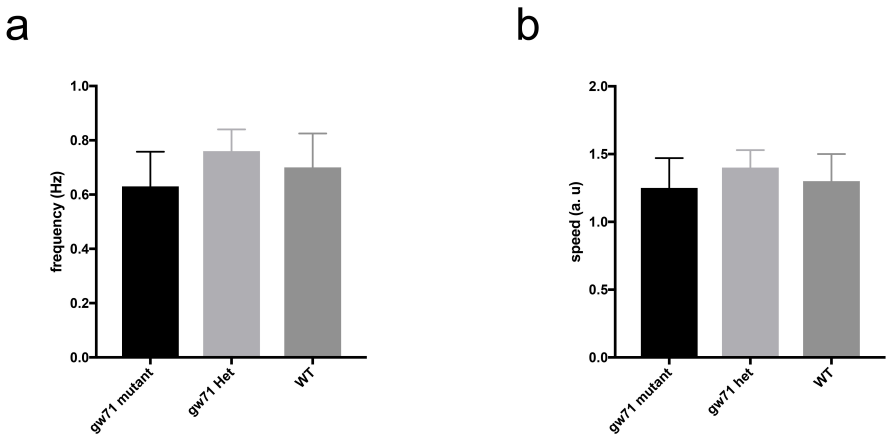

Supplementary Figure 14.

(a) Average activity of WT (black, n=98) and *Cal*^{gw71} mutants (red, n=99), pooled from siblings and cousins, from 5.2 dpf to 6.7 dpf. Light/dark cycle is indicated at bottom. Larvae tested were raised on a 14 h light/10 h dark cycle. For all traces, shaded region is s.e.m. of population.

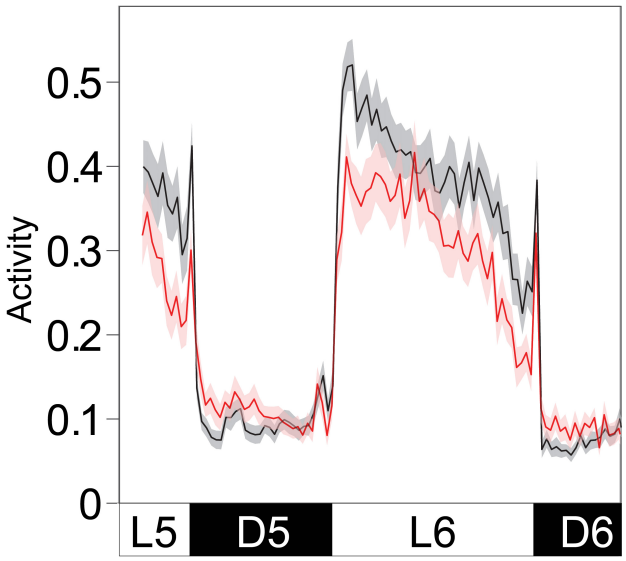

Supplementary Figure 15. Lighting condition does not alter ASR

Plots of circadian ASR tested during the day under light or dark conditions on WT (n=24 for each group). Larvae at 6 dpf were first tested under light condition. After turning off the light and acclimating for a minimum of 30 minutes, larvae were then tested in dark phase. P=0.72 by extra sum-of-squares F test. Bars represent mean ± s.e.m.

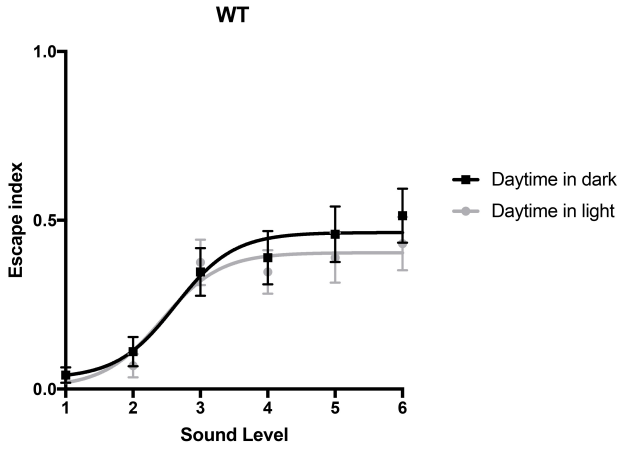

Supplementary Figure 16.

Plots of circadian ASR tested during night (black line) and day (grey line) of 6 dpf WT larvae (a) and *Cal*^{gw71} mutants (b), which are siblings generated from the same cross, identified by genotyping after video recording. Bars represent mean ± s.e.m. WT, N=4; p=0,04. *Cal*^{gw71}

mutants, N=4; p=0.65. Extra sum-of-squares F test. ASR test were performed blindly, followed by genotyping.

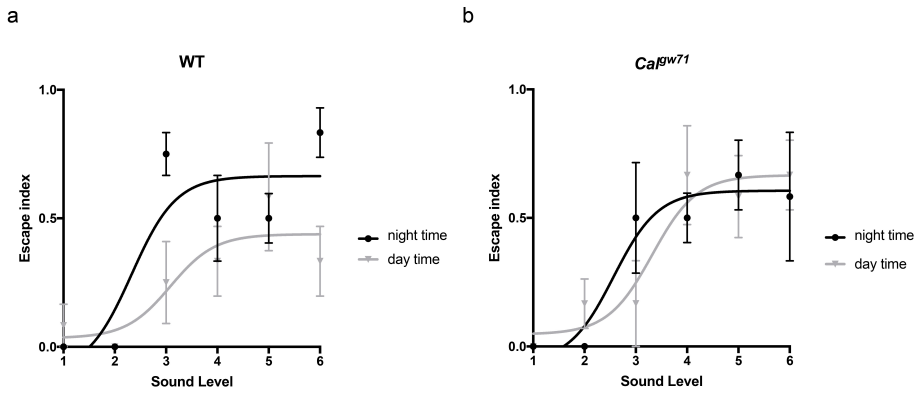

Supplementary Figure 17. Schematic of copper handling mechanism in vertebrate cells. Disruption of copper homeostasis by BCS treatment or Atp7A mutation is indicated. Copper is imported through a high-affinity copper transporter, Ctr1/Slc31A1. A series of metallochaperones then shuttle copper to Atp7A located at the trans-Golgi complex to metalate target proteins. The membrane-impermeable chelator, BCS, chelates free copper from outside of cells.

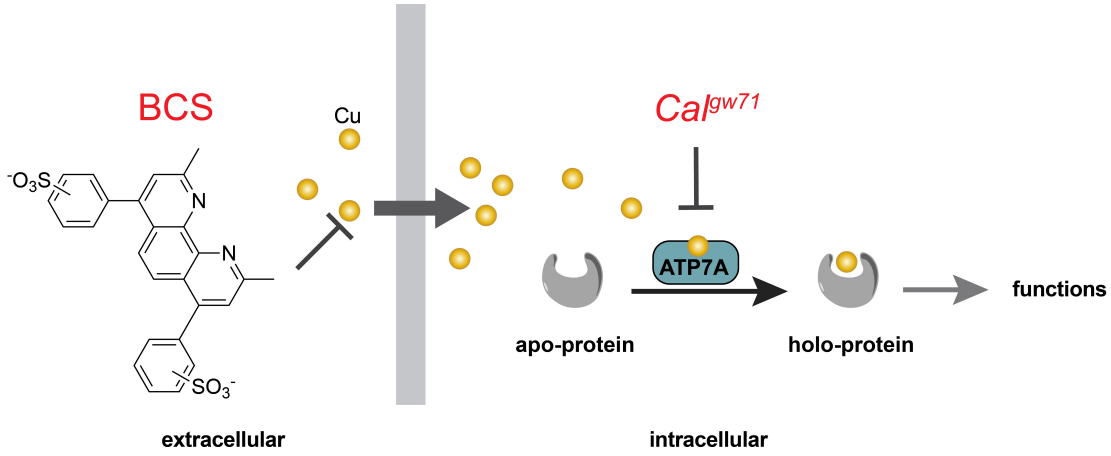

Supplementary Figure 18. BCS treatment does not alter Zn map.

Brain Zn distribution in 6 dpf larval zebrafish analyzed by LA-ICP-MS. (a) and (b) are sections of vehicle-treated wildtype larvae. (c) and (d) are sections of BCS-treated wildtype larvae. N=6 independent animals imaged for each genotype with similar results. Scale bar is 100 μm.

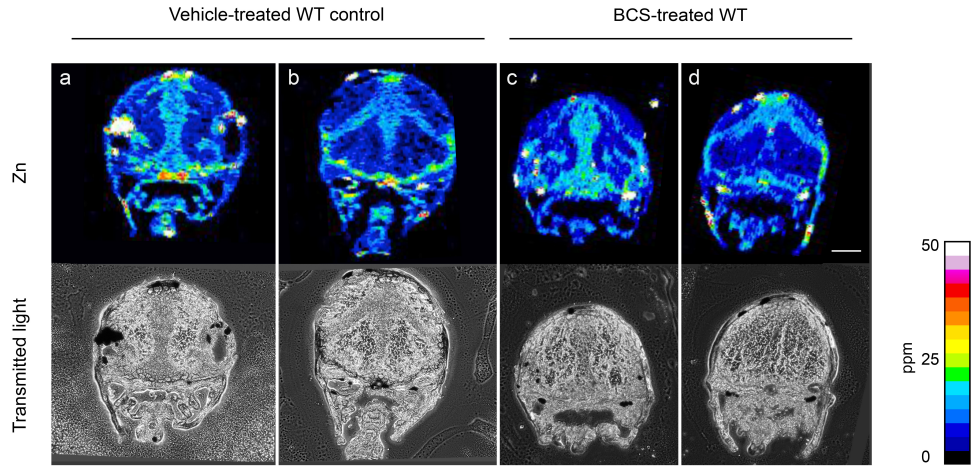

Supplementary Figure 19. CTR1 expression in adult brain

(a) A schematic of adult brain with a line indicates the sections shown in (b) to (c). (b) A coronal section of an adult brain labeled with *in situ* hybridization for ctr1. (c) A coronal section of an adult *Tg(dbh-mCherry)* brain stained with anti-mCherry indicating the somas, in arrows, and neurites, in triangles, of LC neurons.). TeO, optic tectum; CCe, corpus cerebelli. N=3 independent animals imaged for each genotype with similar results. Scale bar is 500 μm.

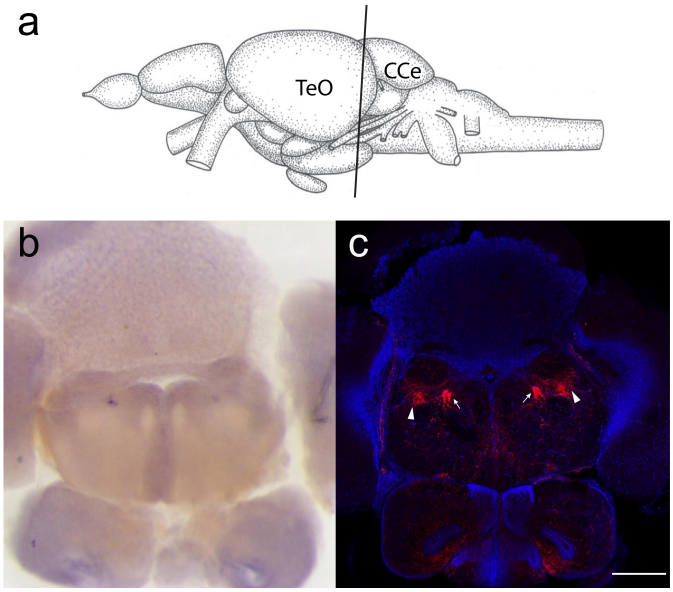

Supplementary Figure 20. LC development through early larval stage.

(a) Dorsal views of a Tg(dbh:mCherry) fish from 2 dpf to 6 dpf. Transmitted-light images show the morphology of brains. Cells in red color are the LC neurons expressing mCherry. N=3 independent animals imaged for each genotype with similar results. Scale bar is 50 μm.

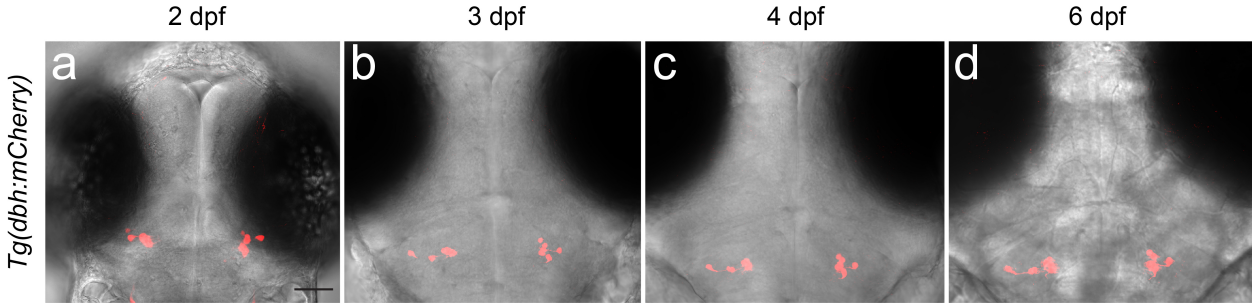

Supplementary Figure 21. LC cell number and distribution is diverse.

(a) Distribution of LC cell numbers in the left brain hemisphere. N=45. (b) Distribution of LC cell numbers in the right brain hemisphere. N=45. (c) A gallery of 20 *Tg(dbh-mCherry)* 4 dpf larvae showing the numbers and patterns of LC neurons.

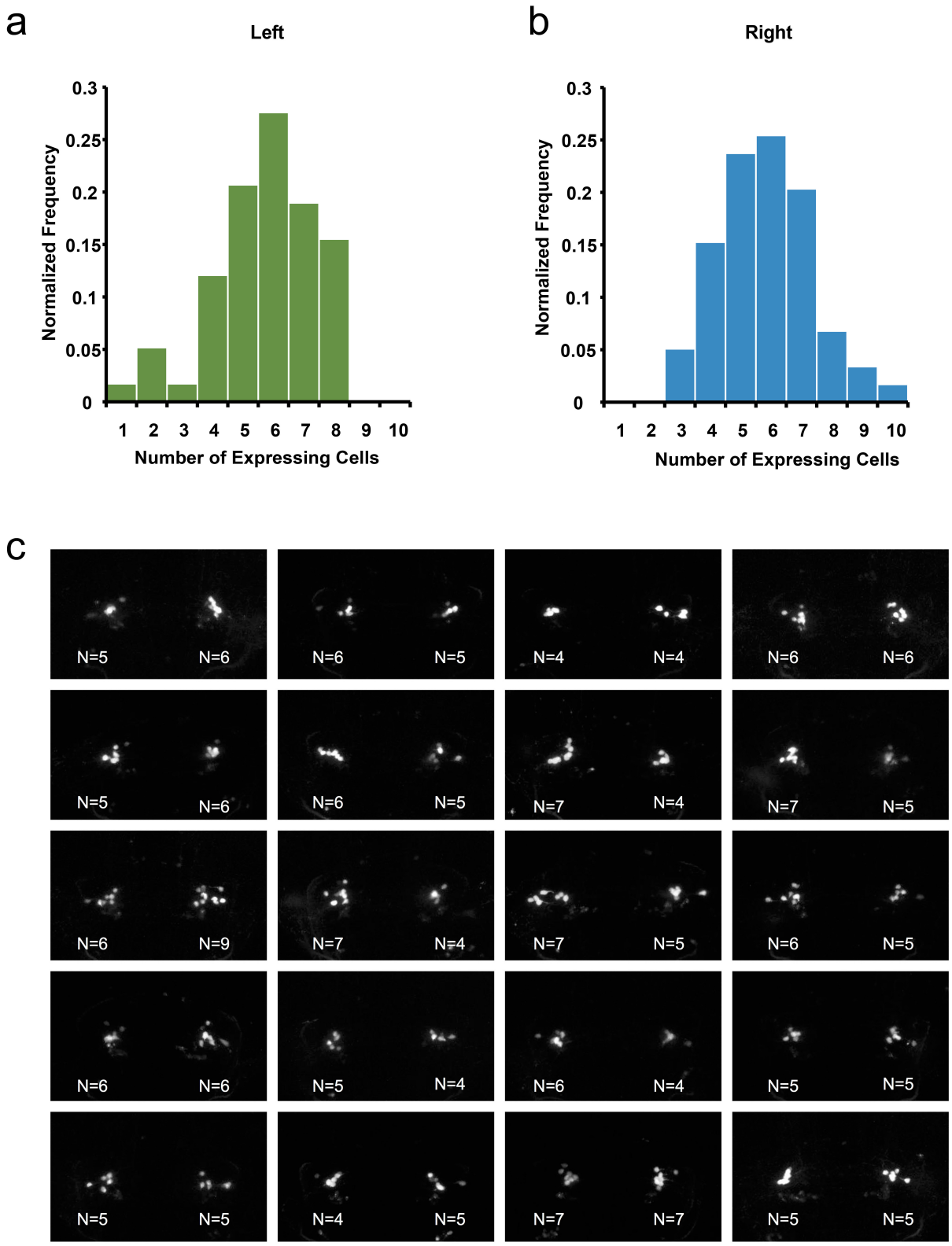

Supplementary Figure 22. LC numbers are asymmetrical in the brain.

Correlation of LC cell numbers from left and right brains. N=12 animals.

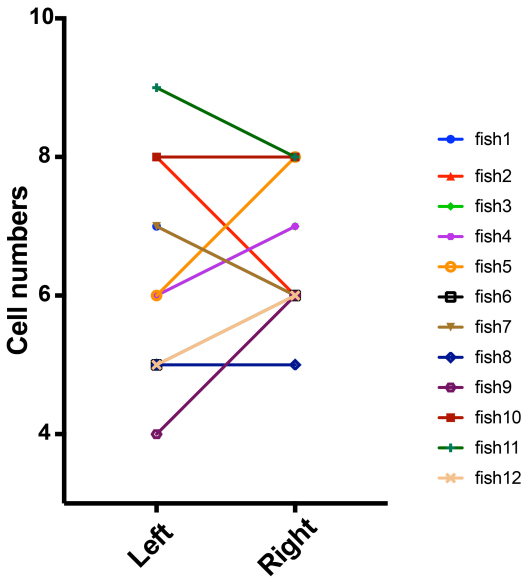

Supplementary Figure 23. The number of LC cells is stable after embryonic neurogenesis.

Average LC numbers over larval development. N=45. Error bars are s.e.m. LC cell numbers remain stable after 3 dpf.

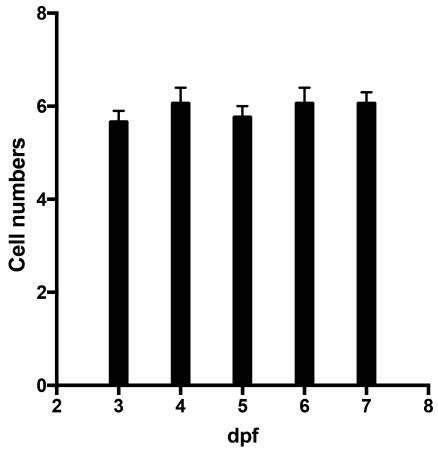

Supplementary Figure 24. The design of laser-ablation analysis.

Schematic showing the design of experiment, in which LC neurons were selectively ablated with 2-photon laser at 3.5-4 dpf. After recovery, behaviors were analyzed from 5-7 dpf. Finally larvae were imaged at 8 dpf to confirm the efficacy of the ablation.

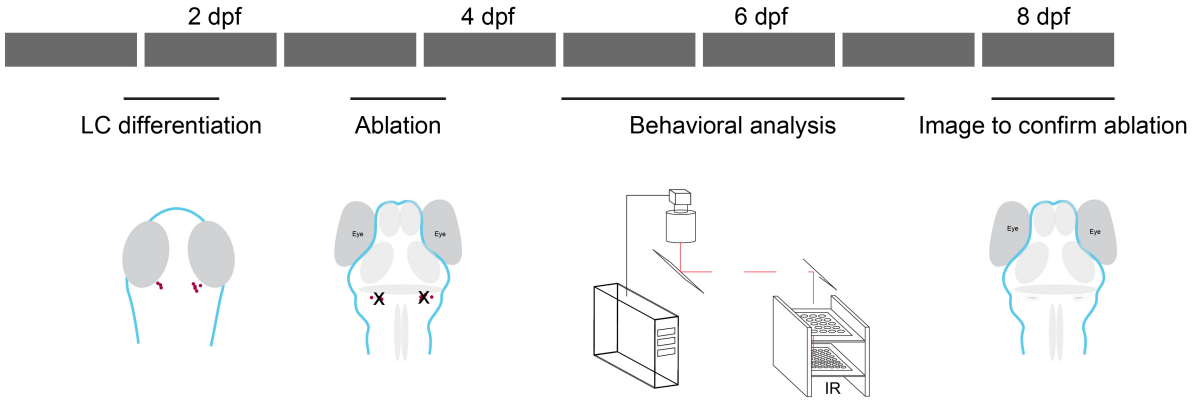

Supplementary Figure 25. 2-Photon laser ablation of the LC

(a) Schematics of 2-photon laser ablation with *Tg(dbh:mCherry)*. (b) Example of selective LC removal by 2-photon laser ablation. Panels show LC cell morphology over time during the ablation process. By the end of ablation, cells are destroyed, and only residual fluorescence remains. (c) and (d) Dorsal views of 8 dpf *Tg(dbh:mCherry*) larvae imaged after behavioral assays. (c) is a sham control fish. (d) is a LC-ablated fish. Scale bar is 50μm.

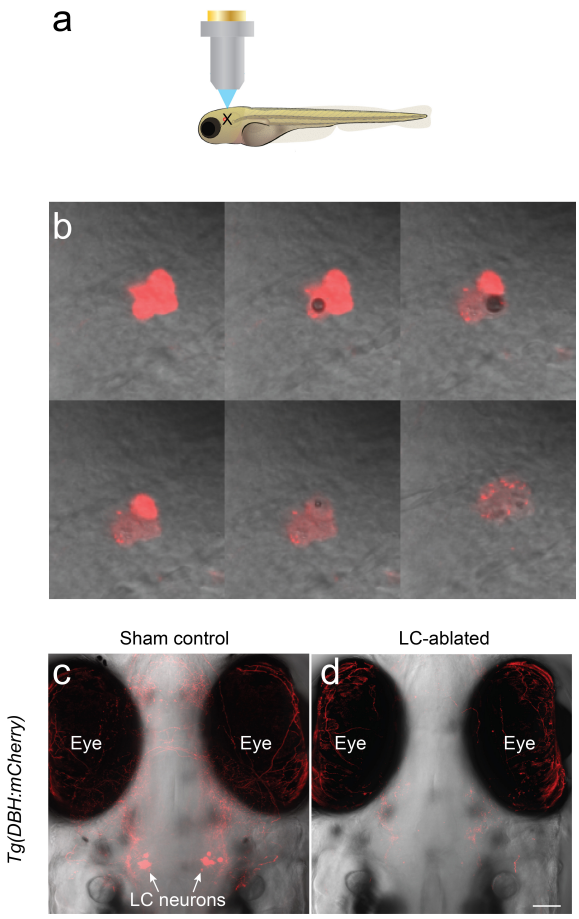

Supplementary Figure 26. Wake-activity roster

(a, b) Activity profiles for all larvae tested between 4 dpf and 6.5 dpf, of thresholded to swim bouts. Light/dark cycle indicated by bar. (a) WT larvae groups: grey = untreated; purple = LC-ablated. (b) *Cal*^{gw71} larvae groups: red = untreated; light blue = 100 nM atomoxetine/SNRI. (c-e) Activity calculated as the number of minutes in which swim bouts occurred per hour during the periods: (c) the night between 4 dpf and 5 dpf; (d), 5 dpf; (e) night between 5 dpf and 6 dpf. Cross represent mean. ***, $p < 0.001$, **, $p < 0.01$; n. s., not significant. Two-sided Student's t-test.

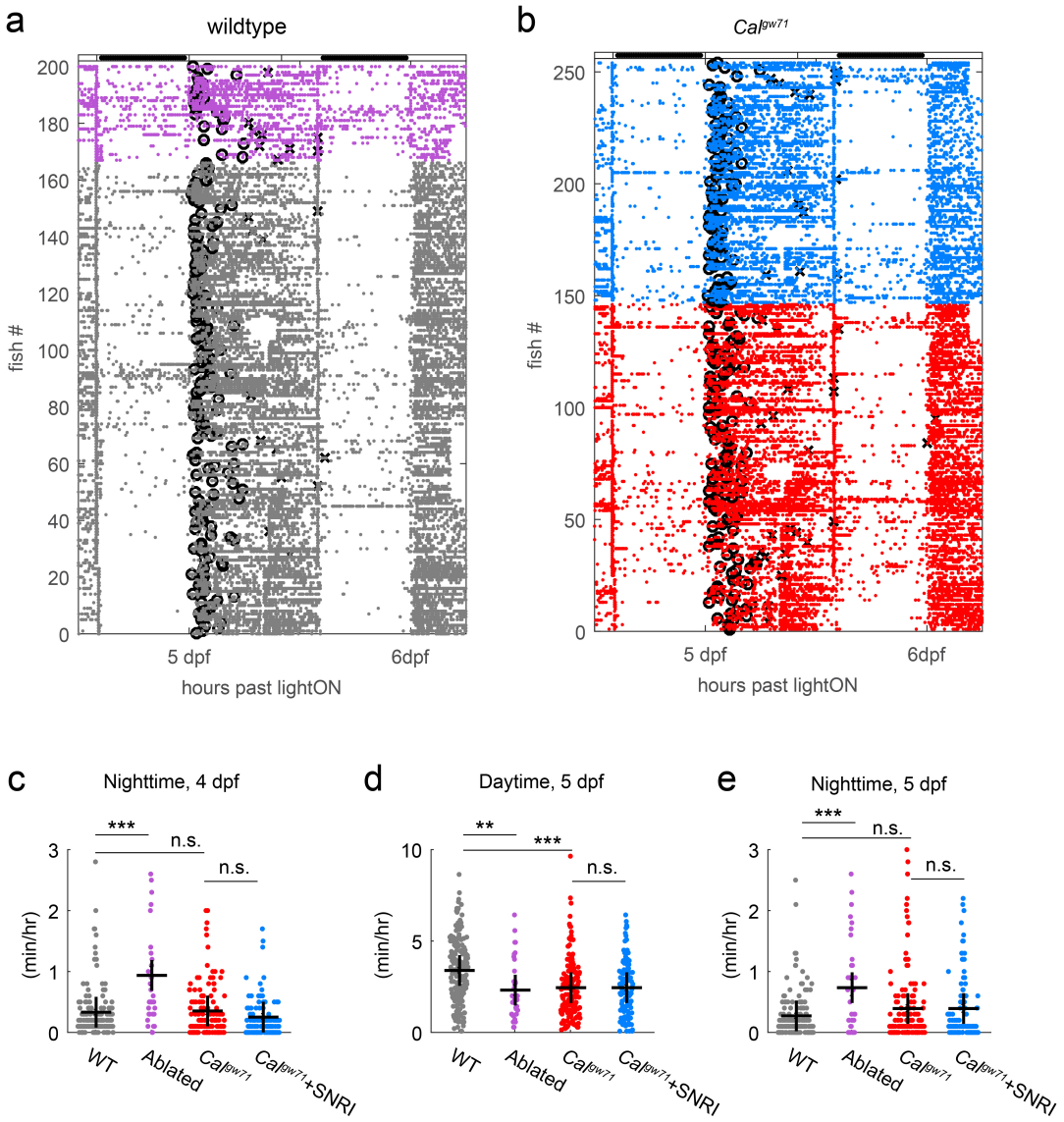

Supplementary Figure 27. Rest-activity cycles of LC-ablated *Cal*^{gw71} mutants

Change in frequency of swim bouts recorded in 3 hr period preceding and following light transitions at dusk and dawn for *Cal*^{gw71} mutants (red, n=63) and LC-ablated *Cal*^{gw71} mutants (green, n=51). Bars represent mean ± s.e.m.

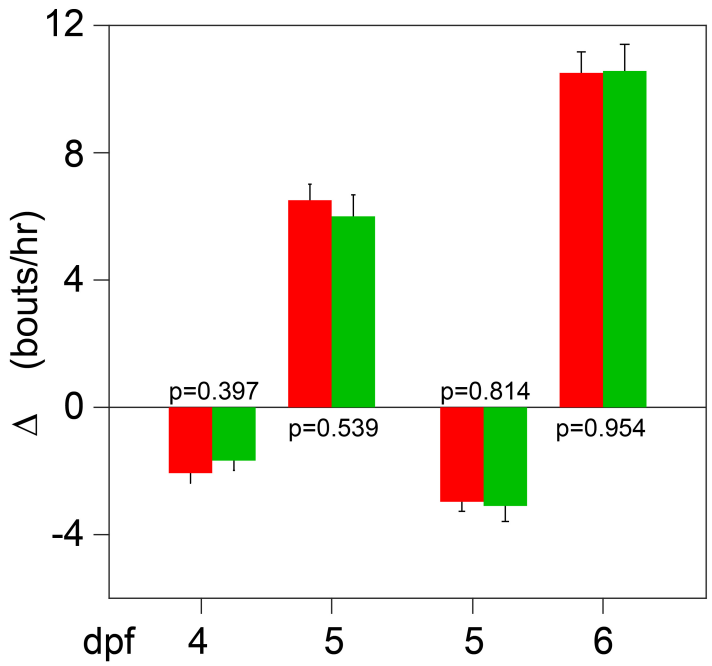

Supplementary Figure 28. dbh mRNA transcription cycles through circadian rhythm.

dbh mRNA expression levels in 6 dpf larvae measured by real-time PCR. Bars represent mean ± s.e.m. The experiment has been repeated independently 3 times with similar results.

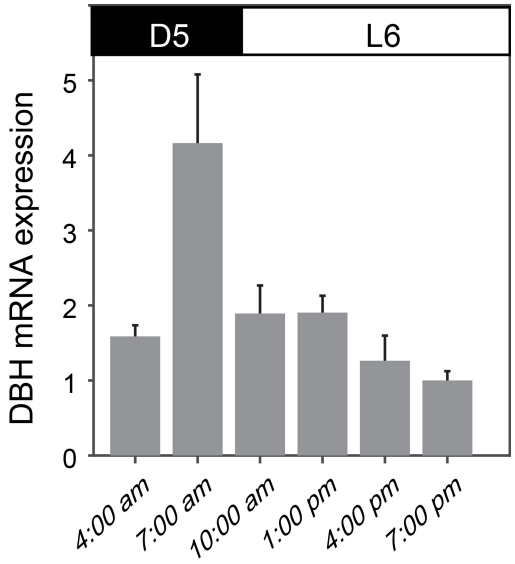

Supplementary Figure 29. ATP7A mRNA transcription is constant during circadian cycles.

ATP7A mRNA expression levels in 6 dpf larvae measured by real-time PCR. Bars represent mean ± s.e.m. The experiment has been repeated independently 3 times with similar results.

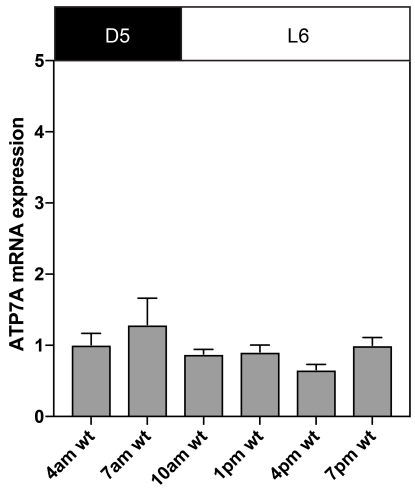

Supplementary Figure 30. DBH expression is unchanged in *Cal*^{gw71} mutants

Dorsal views of 6 dpf larvae labeled with *in situ* hybridization for dbh. (a) and (b) are two examples of wildtype larvae. (c) and (d) are examples of *Cal*^{gw71} mutants. N=12 independent animals labeled in each group with similar results. Scale bar is 50 μm.

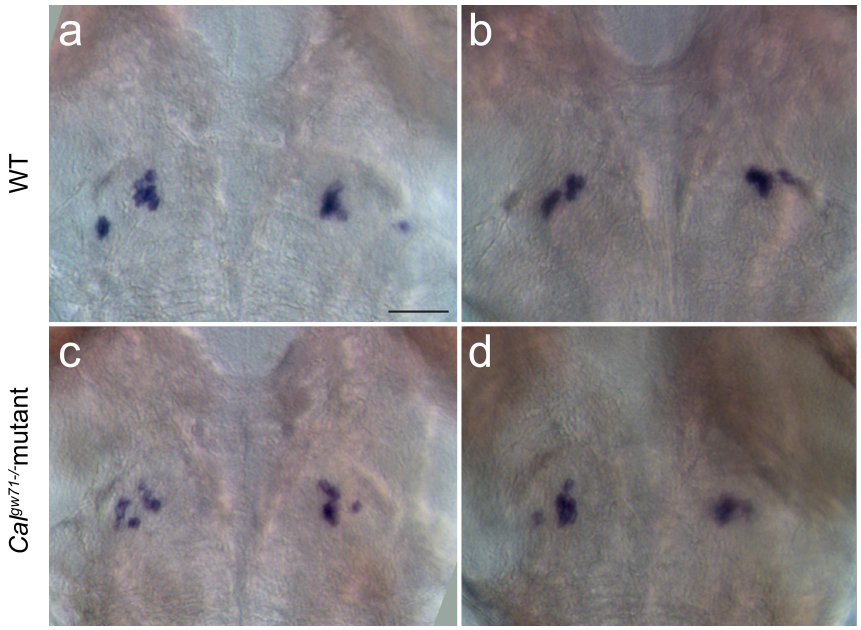

Supplementary Figure 31. NE biosynthesis requires copper

A summary of NE biosynthesis in vertebrates.

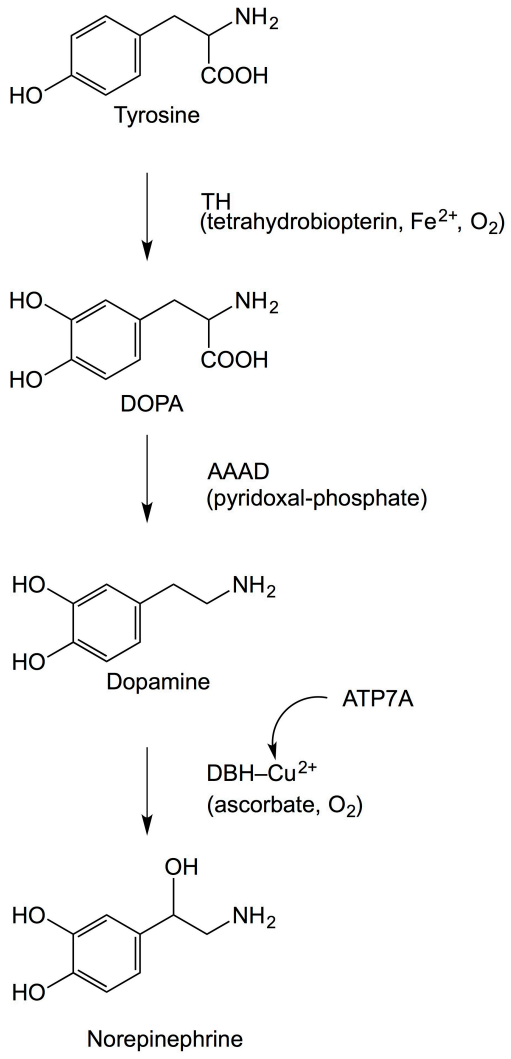

Supplementary Figure 32. Copper transporter gene duplication coincides with the rise of brain NE levels and NE transport in Gnathostomata.

(a) Phylogenetic tree of the atp7 gene family showing the gene duplication event in early chordates, which gave rise to two paralogous genes, atp7a and atp7b, in vertebrates. (b) Phylogenetic tree of the catecholamine transporter gene family. NE transporter (NET/SLC6A2), showing that it results from gene duplications of the DA transporter gene (DAT/SCL6A3) in early chordates. (c) Phylogenetic tree of fish species tested for brain catecholamine levels. (d) NE/DA

ratio in a variety of fish species. N=2 brains for dogfish and stickleback; N=3 brains for all other species. Error bars represent means ± s.e.m.

a

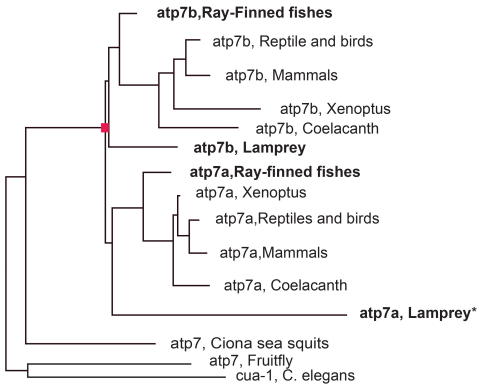

b

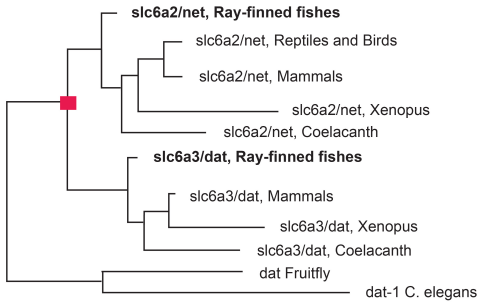

c

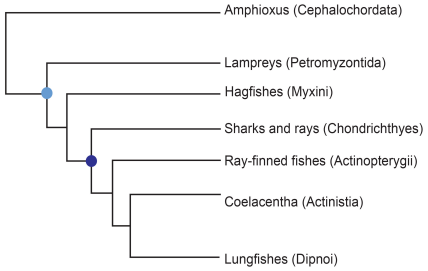

d